

Consistent cell-specific carbon fixation rates by small eukaryotic phytoplankton in contrasting nutrient-limited conditions

Denise Rui Ying Ong ,^{1*} Andrés Gutiérrez-Rodríguez ,^{2,3} Karl A. Safi ,⁴ Dominique Marie,⁵ Karen E. Selph ,⁶ Michael R. Stukel ,^{7,8} Moira Décima ,^{2,9} Adriana Lopes dos Santos ,^{1,10*}

¹Asian School of the Environment, Nanyang Technological University, Singapore, Singapore

²National Institute of Water and Atmospheric Research, Wellington, New Zealand

³Instituto Español de Oceanografía, Centro Oceanográfico de Gijón, Gijón, Spain

⁴National Institute of Water and Atmospheric Research, Hamilton, New Zealand

⁵Sorbonne Université, CNRS, UMR7144, Team ECOMAP, Station Biologique de Roscoff, Roscoff, France

⁶Department of Oceanography, University of Hawai'i at Mānoa, Honolulu, Hawaii, USA

⁷Department of Earth, Ocean and Atmospheric Science, Florida State University, Tallahassee, Florida, USA

⁸Center for Ocean-Atmospheric Prediction Studies, Florida State University, Tallahassee, Florida, USA

⁹Scripps Institution of Oceanography, University of California at San Diego, San Diego, California, USA

¹⁰Department of Biosciences, University of Oslo, Oslo, Norway

Abstract

Small phytoplankton, consisting of pico and nano size fractions, are diverse in size and taxonomy. Yet, the differences in their productivity and taxonomic diversity are poorly described. Here, we measured the cell-specific carbon fixation rates of picocyanobacteria *Synechococcus*, picoeukaryote, and nanoeukaryote populations, while unveiling their taxonomic composition in oligotrophic subtropical and high-nutrient low-chlorophyll subantarctic waters. We coupled 24 h in situ radiolabeled ¹⁴C incubations to flow cytometry sorting and DNA metabarcoding from the same incubated samples, offering a direct account of the community associated with the carbon fixation rates measured. In both water masses, nanoeukaryotes had the highest cell-specific carbon fixation rate, followed by picoeukaryotes and *Synechococcus* (2.24 ± 29.99 , 2.18 ± 2.08 , and 0.78 ± 0.55 fgC cell⁻¹ h⁻¹, respectively). The cell-specific carbon fixation rates and growth rates of *Synechococcus* were three-fold higher in subtropical compared to subantarctic waters, while the rates of picoeukaryotes and nanoeukaryotes had no significant difference between the biogeochemically-contrasting water masses. Sorted picoeukaryote populations were dominated by Mamiellophyceae, Pelagophyceae, Prymnesiophyceae, and Chrysophyceae, while nanoeukaryote populations were dominated by Dinophyceae and Prymnesiophyceae. Despite significant differences in their taxonomic composition, the sorted picoeukaryote populations in subantarctic waters and nanoeukaryote populations in subtropical and subantarctic waters were dominated by taxa reported in the literature as able to engage in phago-mixotrophic strategies (Prymnesiophyceae, Chrysophyceae, and Dinophyceae), suggesting that such trophic strategy might be applied by discrete small photosynthetic eukaryote populations to alleviate macronutrient and iron stress.

*Correspondence: denise.ry.ong@gmail.com; a.l.d.santos@ibv.uio.no

Additional Supporting Information may be found in the online version of this article.

This is an open access article under the terms of the [Creative Commons Attribution](https://creativecommons.org/licenses/by/4.0/) License, which permits use, distribution and reproduction in any medium, provided the original work is properly cited.

Author Contribution Statement: ALS, AG-R, and KAS have contributed to conception and designed. ALS, AG-R, KAS, KES, DRYO, and DM have processed the samples and produced data. DRYO, AG-R, ALS, MRS, KAS, and MD have analyzed and interpreted the data. DRYO drafted the manuscript. All authors have revised and approved the final manuscript.

Marine phytoplankton accounts for half of the Earth's primary production (Field et al. 1998). In the open ocean where low nutrient concentrations prevail, small phytoplankton, which include pico (0.2 to 2–3 μm; Vaulot et al. 2008) and nano (2–3 to 20 μm) size cells as defined in Richardson (2019), are dominant as their lower diffusion boundary layers and higher surface area-to-volume ratio allows a more efficient nutrient acquisition compared to larger phytoplankton (Raven 1998).

Small phytoplankton populations distinguished by size (pico and nano) and taxonomic domains (cyanobacteria and eukaryotes) can exhibit a wide range of primary production rates (C m⁻³ d⁻¹) due to marked differences in cell abundance or

biomass, as well as specific carbon fixation or growth rates. Rate measurements of pico- and nanophytoplankton quantified through combining radiolabeled ^{14}C or stable isotope ^{13}C incubation experiments with size fractionated measurements of the community have shown high contributions of small phytoplankton to primary production (50%–80%) in low nutrient conditions (McKay et al. 2005; Garcia et al. 2007). Flow cytometry sorting can separate the phytoplankton community by cell size and natural photosynthetic pigments, such as phycoerythrin (e.g., picocyanobacteria *Synechococcus* and cryptophytes) and chlorophyll *a* (Chl *a*; e.g., other photosynthetic eukaryotes; Marie et al. 2010). The rate of carbon fixation per cell ($\text{C cell}^{-1} \text{h}^{-1}$) can then be determined by measuring the uptake of isotopic tracers of a given phytoplanktonic population. This can be achieved through direct liquid scintillation counting (cell-specific) of the sorted population (Li 1994; Rii et al. 2016) or more recently (and yet less accessible) at the single-cell level by nanoscale secondary ion mass spectrometry (Berthelot et al. 2019; Irion et al. 2021), to reveal the differences between cell-specific or abundance driving high productivity.

Taxonomic diversity within picocyanobacteria and small photosynthetic eukaryotes can also contribute to the variability in primary production rates. Traits such as cell size, morphology, nutrient requirements and acquisition, and trophic activity (e.g., autotrophy vs. mixotrophy) differ within and between taxonomic lineages (Litchman et al. 2010). Only a few studies using cell-specific or single-cell (nanoscale secondary ion mass spectrometry) approaches have characterized the taxonomic composition of the target phytoplankton community by DNA-based methods, including fluorescence in situ hybridization (Jardillier et al. 2010; Hartmann et al. 2014) and DNA sequencing of marker genes either on the total community (Duerschlag et al. 2021; Irion et al. 2021) or specifically on sorted populations (Rii et al. 2016; Duhamel et al. 2019). Despite differences in productivity (Rii et al. 2016; Irion et al. 2021), and evidence of phylogeography (Farrant et al. 2016; Logares et al. 2020), as well as differences in community composition between pico- and nanoeukaryote assemblages (Obiol et al. 2020), there is still limited information on the influence of taxonomic diversity on productivity of distinct small phytoplankton populations (Rii et al. 2016; Duhamel et al. 2019).

The Southern Ocean is dominated by high-nutrient, low-chlorophyll (HNLC) conditions where primary production is limited by low iron concentrations (Ryan-Keogh et al. 2023), with a growing appreciation for the importance of small phytoplankton in production and export (Irion et al. 2021; Flynn et al. 2023). However, direct measurements of small phytoplankton cell-specific carbon fixation rates have mostly been determined in tropical and subtropical latitudes with mesotrophic and macronutrient-limited conditions (Jardillier et al. 2010; Duerschlag et al. 2021), with only one study thus far conducted in the Southern Ocean comparing iron-limited and

iron-replete conditions (Irion et al. 2021). As macro and micronutrient-limited conditions are expected to intensify at the open ocean surface with climate change (Moore et al. 2018; Ryan-Keogh et al. 2023), characterizing cell-specific carbon fixation rates and taxonomic composition of phytoplankton populations across widespread and contrasting nutrient-limited conditions is paramount to accurately quantify and account for variability in phytoplankton productivity, consequently improving carbon cycle models (Laufkötter et al. 2015).

This study contributes to filling this gap by assessing the relationship between productivity and community composition of small phytoplankton populations in contrasting macro and micro-nutrient limited conditions in subtropical and HNLC subantarctic waters, respectively. Our sampling was conducted across the southern subtropical frontal zone that extends to the east of Aotearoa-New Zealand in the southwest Pacific Ocean, separating biogeochemically distinct subtropical and subantarctic water masses (Boyd et al. 1999). Subtropical waters to the north are warm and nitrogen-limited (Zentara and Kamykowski 1981), while cool subantarctic waters to the south are HNLC (Boyd et al. 1999). We measured cell-specific carbon fixation rates and characterized the taxonomic composition of three small marine phytoplankton populations (picocyanobacteria *Synechococcus*, picoeukaryotes, and nanoeukaryotes) in 24 h in situ radiolabeled ^{14}C incubations coupled to flow cytometry sorting during the austral spring productive season. By quantifying ^{14}C -uptake rates and characterizing taxonomic composition by DNA metabarcoding of the sorted populations sampled from the same incubation bottles, we provide, for the first time, a direct and synoptic account of phytoplankton populations' taxonomic composition and their carbon fixation rates.

Material and methods

Study area and sampling

Sampling was carried out during the Salp Particle expOrt and Oceanic Production (SalpPOOP) cruise on board the R/V *Tangaroa* (TAN1810, 21st October to 21st November 2018), near the Chatham Rise (Décima et al. 2023). The sampling strategy was designed based on Lagrangian experiments (“cycles”), following the same water parcel (Fig. 1a) using a satellite-tracked floating array with a drogue centered at 15 m depth. Profiles of temperature, salinity, fluorescence, and photosynthetically active radiation (PAR) from the water column were obtained with a Seabird (SBE 911plus) CTD (Conductivity-Temperature-Depth) attached to a rosette frame with 10 L Niskin bottles for water collection. Daily variation in incident irradiance was measured at the sea surface with a ship-mounted underway Precision Infrared Radiometer sensor (Eppley; W m^{-2}), and converted to daily integrated incident irradiance measurements ($\text{mol m}^{-2} \text{d}^{-1}$; Fig. S1) via the empirical

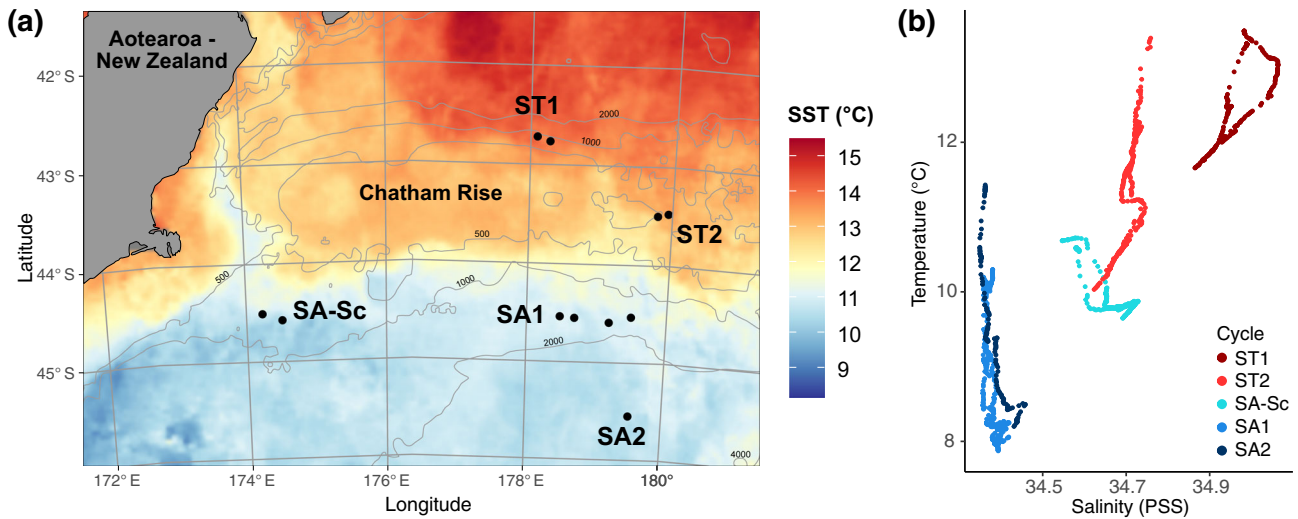


Fig. 1. (a) Map of the study area at the Chatham Rise with monthly average sea surface temperature of November 2018 (NASA MODIS satellite). Each point represents one ^{14}C incubation experiment within a cycle in subtropical (ST) and subantarctic (SA) waters. (b) Temperature-salinity plot of each cycle obtained from downcast CTD measurements from 0 to 150 m depth.

relationship between parallel measurements from the Eppley radiometer and PAR radiometer. Each experimental cycle was sampled for periods of 3–5.5 d, with two conducted in subtropical waters (ST1 and ST2) and three in subantarctic waters (SA-Sc, SA1, and SA2; Fig. 1a; Décima et al. 2023). Water samples were obtained from daily pre-dawn CTDs (02:00 deployment) to (1) conduct ^{14}C -uptake experiments, (2) obtain phytoplankton cell abundances and forward scatter (FSC) measurements by flow cytometry, and (3) determine total community taxonomic composition by DNA sequencing. Morning CTDs (09:00–12:00 h deployment) were obtained from several depths (Table S1) to measure nutrient and size-fractionated Chl *a* concentration as described in Décima et al. (2023, see Supporting Information for details).

Flow cytometry

After cell-specific incubations (see ^{14}C -fixation rates section below), seawater samples preserved in glutaraldehyde (^{14}C -uptake measurements) or DMSO (DNA sequencing; together with preserved seawater samples obtained during initial sampling from the same CTD casts) were sorted to obtain *Synechococcus*, picoeukaryote, and nanoeukaryote populations using FACSAria™ flow cytometer (Becton-Dickinson, P07800142) as described in the Supporting Information (Tables S2, S3). Additional aliquots of seawater taken from the same CTD casts used for cell-specific rate incubations were (1) preserved in paraformaldehyde (Electron Microscopy Sciences 157-4, 0.5% final concentration) for later shore-based analyses on a CytoFlex S flow cytometer (Beckman Coulter) after staining with Hoechst 34580 (Sigma-Aldrich 63493; Selph 2021), for *Synechococcus* enumeration, and (2) analyzed within 1–2 h,

unpreserved, for eukaryotic phytoplankton cell enumeration and FSC signals (all populations) using a shipboard Accuri C6 Plus flow cytometer (Becton-Dickinson, BD 661311) as described in Stukel et al. (2021).

^{14}C -fixation rates

Small phytoplankton cell-specific carbon fixation rates and volumetric net primary production (NPP) rates were measured by ^{14}C -uptake during 24-h in situ incubation experiments, where the spiked seawater was incubated at the corresponding depths sampled. Cell-specific experiments were conducted in the surface mixed layer (12 m) and the deep chlorophyll maximum (DCM; from 25 to 70 m), while standard volumetric NPP experiments were carried out at 6 depths, from 5 m to below the DCM (from 50 to 100 m), with specific depths of each cycle presented in Table S1. Cell-specific and volumetric NPP experiments were conducted between one and four times in each experimental cycle, yielding a total of 11 and 17 rate profiles, respectively.

For cell-specific carbon fixation rate measurements, seawater from each depth was spiked with ^{14}C -sodium bicarbonate (Perkin Elmer, NEC086H005MC) at $203.5 \text{ kBq mL}^{-1}$ final concentration and distributed into four gas tight borosilicate vials (8 mL, JG Finneran, 88020-1760; 3 light + 1 dark control) to a total volume of 7.4 mL. Two sets of duplicates of 1.5 mL seawater were taken from each vial after incubation for ^{14}C -uptake measurements and DNA sequencing, preserved with glutaraldehyde (Sigma-Aldrich G6257, 1% final concentration) and DMSO (Sigma-Aldrich D8418, 10% final concentration), respectively. All samples were stored at -80°C until fluorescence-activated cell sorting by flow cytometry. See Supporting Information for details.

Volumetric NPP experiments with standard volume incubations (320 mL) were conducted as described in Décima et al. (2023). To evaluate the impact of a smaller volume incubation used for cell-specific measurements, small volume incubations (7.4 mL) for NPP measurements at surface and DCM depths were also obtained (Fig. S2), as described in the Supporting Information.

The radioactivity retained in cells for cell-specific and volumetric NPP measurements were measured as disintegrations per minute (DPM) using a Liquid Scintillation counter (Beckman Coulter, LS6500) as described in Gutiérrez-Rodríguez et al. (2020). Disintegrations per minute from the dark incubation was subtracted from the light incubation to account for light independent carbon fixation. Disintegrations per minute for volumetric NPP was converted to mmolC m⁻³ d⁻¹ using volume, total added activity, and measured dissolved inorganic carbon concentrations (Gutiérrez-Rodríguez et al. 2020). The volumetric NPP rates were integrated across the six depths using a trapezoidal integration.

To obtain cell-specific carbon fixation rates of different groups, three quantities of 2000, 4000, and 10,000 cells belonging to *Synechococcus* and picoeukaryotes populations were sorted from each vial to quantify the total DPM (Table S2). Disintegrations per minute per cell was then calculated using type I linear regression. For nanoeukaryotes, the average DPM per cell was calculated from 1000 cells for each vial. Disintegrations per minute per cell from dark vials were subtracted from light vials. Cell-specific carbon fixation rates (fgC cell⁻¹ h⁻¹) were calculated based on DPM per cell as follows:

$$\text{Cell-specific CO}_2 \text{ fixation} = \text{DIC} \times \frac{\text{DPM}_{\text{cell}}}{\text{SA} \times 24} \times 1.05 \times 10^9$$

where DIC = dissolved inorganic carbon (mgC L⁻¹), DPM_{cell} = DPM per cell after incubation for 24 h as calculated from above, SA = standard activity in 1 mL (DPM per mL). Twenty-four is used to convert units from day⁻¹ to h⁻¹, 1.05 is used to account for the differential uptake between ¹⁴C and ¹²C, and 10⁹ is used to convert between units from L to m³ and from mg to fg.

We excluded measurements from experiment 7 in ST1 from the analysis due to uncertainty in the values of DPM. Raw measurements are reported in the Supporting Information (Figs. S3–S6).

Group-specific productivity (mgC m⁻³ d⁻¹) was calculated by multiplying cell-specific carbon fixation rates with cell abundance measured by flow cytometry in seawater samples from the same CTD cast and depth used for ¹⁴C-bicarbonate incubation (Fig. S6).

Growth rates

We estimated cell diameter (μm) and subsequently cell biovolume (BV; μm³), assuming spherical shape, of

unpreserved *Synechococcus*, photosynthetic picoeukaryotes and nanoeukaryotes from average FSC cytometric signal at each corresponding incubation and depth, normalized to polystyrene reference beads (Polysciences, Warrington, PA). The average carbon biomass per cell (C; pgC cell⁻¹) of each photosynthetic population was calculated based on BV using the conversion factor of $C = \text{BV} \times 0.265 \text{ pgC } \mu\text{m}^{-3}$ for *Synechococcus* (Bertilsson et al. 2003), and $C = 0.216 \times \text{BV}^{0.939}$ for eukaryotic cells (Menden-Deuer and Lessard 2000).

Growth rate (day⁻¹) was calculated for each vial from the ¹⁴C-bicarbonate incubation as follows:

$$\text{Growth rate (day}^{-1}\text{)} = \frac{\text{Cell-specific CO}_2 \text{ fixation (pg cell}^{-1}\text{h}^{-1}\text{)}}{\text{Carbon biomass per cell (pg cell}^{-1}\text{)}} \times 24$$

DNA extraction, PCR, and amplicon analysis

Seawater volumes of 1.4–2.4 L were filtered through a 0.22 μm pore-size Sterivex filter (Millipore), flash frozen in liquid nitrogen, and stored at –80°C until processed (Table S4). DNA from filtered seawater was extracted using the DNeasy mini Blood and Tissue Kit (Qiagen, Germany). DNA from the sorted cells was extracted using three cycles of flash-freezing and thawing in liquid nitrogen (Table S3; Gérikas Ribeiro et al. 2018).

PCR was performed using the following primer sets: Nested PCR targeting *petB* gene of *Synechococcus* for filtered and sorted samples, *petB*-F (5'-TACGACTGGTTCAGGAACG-3') and *petB*-634R (5'-GCTTVCGRATCATCARGAAG-3'), followed by *petB*-50F (5'-TYCAGGACATYGCTGAY-3') and *petB*-R (5'-GAAGTGCA TGAGCATGAA-3'; Ong et al. 2023); nested PCR targeting 18S rRNA (V4 hypervariable region) for sorted picoeukaryotes and nanoeukaryotes samples (Gérikas Ribeiro et al. 2018), 63F (5'-ACGCTTGCTCAAAGATTA-3') and 1818R (5'-ACGGAAAC CTTGTTACGA-3'), followed by TAREuk454FWD1 (5'-CCA GCASCYCGGTAATTCC-3') and V4 18S Next. Rev (5'-ACTTTCGTTCTTGATYRATGA-3'); 18S rRNA seawater samples, TAREuk454FWD1 and V4 18S Next. Rev (Piredda et al. 2017). Samples were purified, barcoded, and sequenced using the Illumina MiSeq platform 2 × 300 bp for *petB* and 2 × 250 bp for 18S rRNA. Detailed protocols of PCR conditions are reported in the Supporting Information.

Sequence data was processed on RStudio Version 1.4.1717 using DADA2 R package Version 1.12 (Callahan et al. 2016). Taxonomy was assigned against a *petB* reference sequence database (Farrant et al. 2016) for *Synechococcus*, and PR² database version 4.14 (Guillou et al. 2013) for eukaryotes. Amplicon sequence variants (ASVs) were classified based on trophic mode (phototrophic, phago-mixotrophic, or heterotrophic) based on the Schneider et al. (2020) database and updated with recent gene-based model predictions for Prymnesiophyceae (Koppelle et al. 2022; full list of trophic

assignment on [Github](#)). Amplicon sequence variants without a trophic mode assignment or unclassified at species level were assigned based on a “majority rule” approach, where the assignment was based on the most abundant trophic mode of a given taxon (Sim et al. 2024). Amplicon sequence variants assigned to Supergroup Opisthokonta, Division Metazoa, Fungi and Pseudofungi, class Syndiniales, as well as protists assigned as heterotrophic were removed and not considered in this study. The trophic mode classification (only phototrophic or phagomixotrophic) of abundant species (i.e., median relative abundance higher than 5% of total reads within each sorted population for any cycle) in the sorted pico and nanoeukaryote populations can be found in Table S5. The community composition from initial sampling was similar to that of light and dark incubation after 24 h for all three populations (Figs. S7–S9). Therefore, only samples from light incubation were used to analyze the sorted phytoplankton community. Details are provided in the Supporting Information.

Statistical analysis

We built three linear models with cell-specific carbon fixation rates, group-specific productivity, or growth rates as a response variable to test for significant differences between phytoplankton group and water masses using ANOVA. All models were simplified by backward deletion ($p < 0.05$). All estimated marginal means (i.e., computed means based on the statistical model) with 95% confidence intervals from model outputs are summarized in Table S6. See Supporting Information for details.

Results

Phytoplankton biomass, abundance, and net primary production

Subtropical cycles were warmer (12–13°C), more saline (34.7–35 ps), and had lower macronutrient concentrations compared to subantarctic cycles (10–11°C; 34.4–34.7 psu; Figs. 1, S10), while SA-Sc cycle showed intermediate characteristics (Fig. 1b) likely reflecting the influence of the Southland Current, a coastal expression of the Subtropical Front that transport northwards a mix of neritic subtropical and subantarctic waters.

Integrated volumetric NPP and Chl *a* concentrations were on average higher in subtropical than in subantarctic cycles (mean \pm SD; NPP: 603.9 \pm 294.9 and 370.5 \pm 194.9 mgC m⁻² d⁻¹; Chl *a*: 58.5 \pm 24.3 and 43.6 \pm 25.7 mg m⁻², respectively), except SA-Sc with similar NPP and Chl *a* concentrations to subtropical cycles (Fig. S11).

Chlorophyll *a* biomass in all cycles was dominated by picoplankton (0.2–2 μ m), which contributed to at least 43% of Chl *a*, followed by nanophytoplankton (2–20 μ m) which accounted for 21%–39% of Chl *a* (Fig. S12). Microphytoplankton (> 20 μ m) had the lowest proportion of Chl *a* across all the cycles (5%–17%), except in SA-Sc where it accounted for 31% of it.

Overall phytoplankton abundances were dominated by *Synechococcus*, followed by picoeukaryotes and nanoeukaryotes (53.7 \pm 35.5, 14.6 \pm 7, and 1.8 \pm 0.7 $\times 10^3$ cells mL⁻¹, respectively; Table 1; Fig. S10). Photosynthetic pico- and nanoeukaryotes abundances were slightly higher in subtropical compared to subantarctic cycles (Table 1;

Table 1. Cell-specific carbon fixation rates, group-specific productivity, cell abundance, and carbon-fixation-based growth rates (mean \pm SD) for *Synechococcus* (Syn), Picoeukaryotes (Pico), and Nanoeukaryotes (Nano) at each cycle in subtropical (ST) and subantarctic (SA) waters. The number of samples for each cycle and group is stated in brackets beside carbon fixation values.

Group	ST1	ST2	SA-Sc	SA1	SA2
Cell-specific CO ₂ fixation (fgC cell ⁻¹ h ⁻¹)					
Syn	1.04 \pm 0.99 (3)	1.41 \pm 0.30 (11)	0.25 \pm 0.14 (5)	0.56 \pm 0.27 (15)	0.32 \pm 0.09 (5)
Pico	2.57 \pm 3.32 (3)	2.29 \pm 0.73 (11)	0.40 \pm 0.21 (5)	2.94 \pm 2.80 (15)	1.37 \pm 0.79 (6)
Nano	29.27 \pm 12.60 (3)	55.96 \pm 22.98 (11)	40.58 \pm 5.66 (6)	67.60 \pm 37.28 (16)	27.60 \pm 7.72 (6)
Cell abundance ($\times 10^3$ cells mL ⁻¹)					
Syn	83.98	16.03 \pm 4.79	31.87 \pm 5.83	67.15 \pm 21.69	42.80 \pm 31.26
Pico	19.41	12.81 \pm 5.09	24.36 \pm 0.60	11.44 \pm 2.10	6.25 \pm 3.18
Nano	2.22	1.77 \pm 0.84	1.43 \pm 0.33	2.38 \pm 0.30	1.16 \pm 0.52
Group-specific productivity (mgC m ⁻³ d ⁻¹)					
Syn	2.10 \pm 1.99	0.55 \pm 0.23	0.18 \pm 0.08	0.89 \pm 0.55	0.27 \pm 0.12
Pico	1.20 \pm 1.55	0.64 \pm 0.23	0.23 \pm 0.12	0.88 \pm 0.97	0.15 \pm 0.02
Nano	1.56 \pm 0.67	2.64 \pm 1.94	1.40 \pm 0.40	3.97 \pm 2.45	0.84 \pm 0.55
C-based growth rate (day ⁻¹)					
Syn	0.19 \pm 0.18	0.29 \pm 0.10	0.06 \pm 0.03	0.11 \pm 0.06	0.07 \pm 0.02
Pico	0.29 \pm 0.37	0.29 \pm 0.10	0.07 \pm 0.03	0.30 \pm 0.29	0.17 \pm 0.09
Nano	0.10 \pm 0.04	0.33 \pm 0.19	0.32 \pm 0.12	0.34 \pm 0.19	0.17 \pm 0.03

Fig. S10I–J) and higher at surface compared to DCM (Fig. S10I–J), although these differences were not statistically significant (Table S7; $p > 0.1$). *Synechococcus* was significantly more abundant in subantarctic compared to subtropical cycles ($t_{12} = -2.2072$, $p = 0.05$), and more abundant (although not statistically significant; $p = 0.6$; Table S7) at DCM compared to surface depths (Table 1; Fig. S10H).

Cell-specific carbon fixation rates and group-specific productivity

Cell-specific carbon fixation rates ($\text{fgC cell}^{-1} \text{h}^{-1}$) and group-specific productivity ($\text{mgC m}^{-3} \text{d}^{-1}$) had high variability among replicates and incubations within the same cycle, with differences of up to one order of magnitude in a few experiments (Figs. S3, S4). Despite this variability, significant differences in both rate measurements emerged between phytoplankton groups and water masses. Conversely, there were no significant differences between surface and DCM for both cell-specific carbon fixation rates and group-specific productivity for any of the phytoplankton groups analyzed ($p \geq 0.13$; Table S7). Therefore, the rate measurements from the two depths have been combined in the following results.

Mean cell-specific carbon fixation rate was highest for nanoeukaryotes, intermediate for picoeukaryotes, and lowest for *Synechococcus* (52.24 ± 29.99 , 2.18 ± 2.08 , and 0.78 ± 0.55 $\text{fgC cell}^{-1} \text{h}^{-1}$, respectively; Table 1). There was a significant interaction between phytoplankton group and water mass on cell-specific carbon fixation rates (Fig. 2a). In subtropical cycles, the cell-specific carbon fixation rate of nanoeukaryotes was significantly higher than that of *Synechococcus* and

picoeukaryotes ($p < 0.0001$), although differences between these picoplanktonic groups were not statistically significant ($p = 0.44$; Fig. 2a; Table S6). In subantarctic cycles, nanoeukaryotes had the highest cell-specific carbon fixation rates, followed by picoeukaryotes and *Synechococcus*, with all three groups showing statistically significant differences ($p < 0.0001$; Fig. 2a; Table S6). The cell-specific carbon fixation rate of *Synechococcus* was three times higher in subtropical compared to subantarctic cycles based on the estimated marginal means ($p < 0.0001$), while there was no significant difference between the rates in subtropical and subantarctic cycles for photosynthetic eukaryotes ($p > 0.37$; Fig. 2a; Table S6).

Mean group-specific productivity was highest for nanoeukaryotes, intermediate for *Synechococcus*, and lowest for picoeukaryotes (2.64 ± 2.16 , 0.78 ± 0.80 , and 0.65 ± 0.76 $\text{mgC m}^{-3} \text{d}^{-1}$, respectively; Table 1). Nanoeukaryotes had the highest group-specific productivity across all cycles, except in ST1, where *Synechococcus* had the highest productivity (Table 1). There was a significant difference in group-specific productivity between phytoplankton populations (Fig. 2b). Nanoeukaryotes showed significantly higher group-specific productivity than both *Synechococcus* and picoeukaryotes with the estimated marginal means around three times higher ($p < 0.0001$), while differences were not statistically significant between the picophytoplankton groups ($p = 0.37$; Fig. 2b; Table S6). There was no significant difference in group-specific productivity between water masses (Fig. 2b; Table S6).

Carbon-based growth rates and cell biovolume

Mean growth rate was highest for nanoeukaryotes, intermediate for picoeukaryotes, and lowest for *Synechococcus*

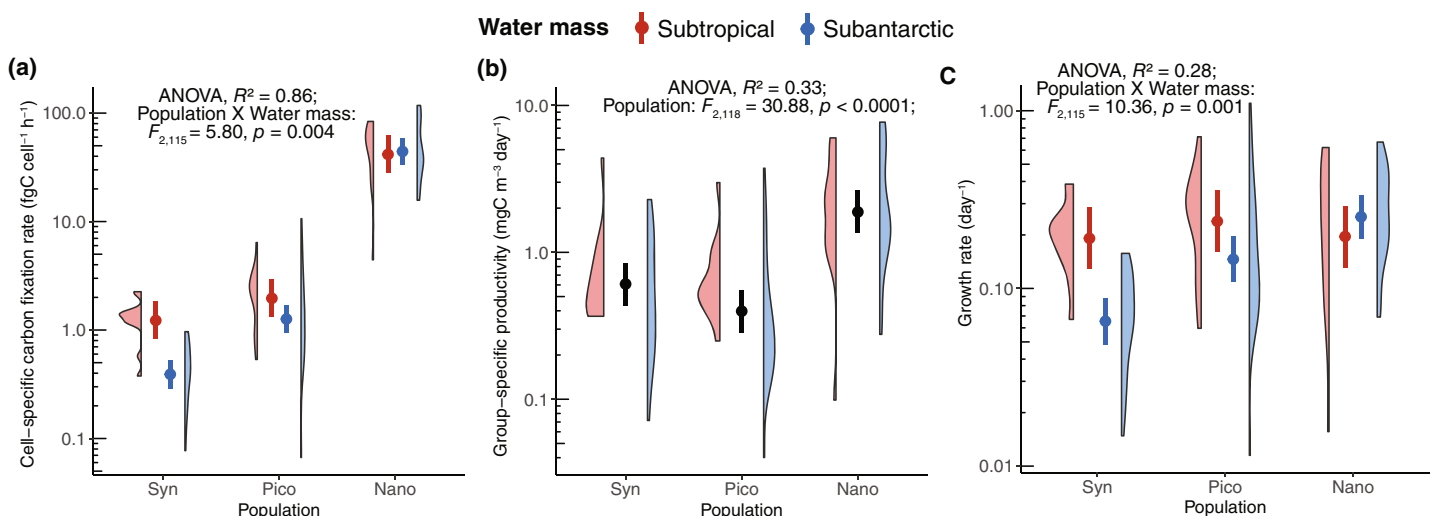


Fig. 2. (a) Cell-specific carbon fixation rate ($\text{fgC cell}^{-1} \text{h}^{-1}$), (b) group-specific productivity ($\text{mgC m}^{-3} \text{d}^{-1}$), and (c) carbon-fixation-based growth rate (day^{-1}) of *Synechococcus* (Syn), picoeukaryotes (Pico), and nanoeukaryotes (Nano) populations. The violin plot shows the distribution of individual measurements, and the point-range plot represents the estimated marginal mean (EMM; dot) and 95% confidence interval (CI; line) of the model. There was no significant difference in group-specific productivity between water masses, therefore EMM and CI presented in (b) account for population only.

(0.29 ± 0.17 , 0.24 ± 0.22 , and $0.13 \pm 0.09 \text{ d}^{-1}$, respectively; Table 1; Fig. S5). There were no significant differences in growth rates between surface and DCM for any of the phytoplankton groups analyzed ($p \geq 0.07$; Table S7). Therefore, the rate measurements from the two depths have been combined in the following results.

There was a significant interaction between phytoplankton group and water mass on growth rates (Fig. 2c). In subtropical cycles, there was no significant difference in the growth rate between the groups ($p > 0.90$; Fig. 2c; Table S6). In subantarctic cycles, nanoeukaryotes had the highest growth rates ($p < 0.05$), followed by picoeukaryotes and *Synechococcus* ($p = 0.001$), with all three groups showing significant differences (Fig. 2d; Table S6). The growth rate of *Synechococcus* was significantly higher in subtropical than subantarctic cycles ($p = 0.0002$), while the growth rate of pico- and nanoeukaryotes were not significantly different between the water masses ($p > 0.25$; Table 1).

Cell diameter, and therefore cell biovolume, for each phytoplankton group was not significantly different between water mass (subtropical and subantarctic cycles) and depth (surface and DCM; Table S7), suggesting observed differences in growth rates reflected physiological rates rather than cell size changes. Mean cell diameter of *Synechococcus*, picoeukaryotes, and nanoeukaryotes were 1.0 ± 0.05 , 1.2 ± 0.07 , and $3.61 \pm 0.59 \mu\text{m}$, respectively.

Phytoplankton community composition

All three sorted phytoplankton populations were structured by water mass (Fig. 3) with significant differences in the community composition observed between subtropical and subantarctic cycles (PERMANOVA-Adonis; *Synechococcus*, $R^2 = 0.18$, $p = 0.001$; picoeukaryotes, $R^2 = 0.24$, $p = 0.001$; nanoeukaryotes, $R^2 = 0.18$, $p = 0.001$). The eukaryotic phytoplankton community was also structured by size (Fig. 3b), where the community composition of picoeukaryotes was significantly different from that of nanoeukaryotes (PERMANOVA-Adonis; $R^2 = 0.26$, $p = 0.001$). There were no significant differences in the community composition between surface and DCM (PERMANOVA-Adonis; *Synechococcus*, $R^2 = 0.03$, $p = 0.06$; picoeukaryotes, $R^2 = 0.02$, $p = 0.163$; nanoeukaryotes, $R^2 = 0.03$, $p = 0.07$).

Overall, the more abundant classes (i.e., taxa with median relative abundance higher than 5% of total reads within each sorted population for any cycle) present in pico and nanoeukaryote sorted populations were distinct, except for Prymnesiophyceae present in both populations (Fig. 4a–c). Within picoeukaryotes, Mamiellophyceae was the most abundant class contributing to 63.0% of total reads, followed by Pelagophyceae (12.4%), Prymnesiophyceae (11.0%) and Chrysophyceae (7.6%; Fig. 4a). The median relative abundance of Mamiellophyceae in subtropical cycles (85.8%) was twice that of oceanic subantarctic cycles (36.6%),

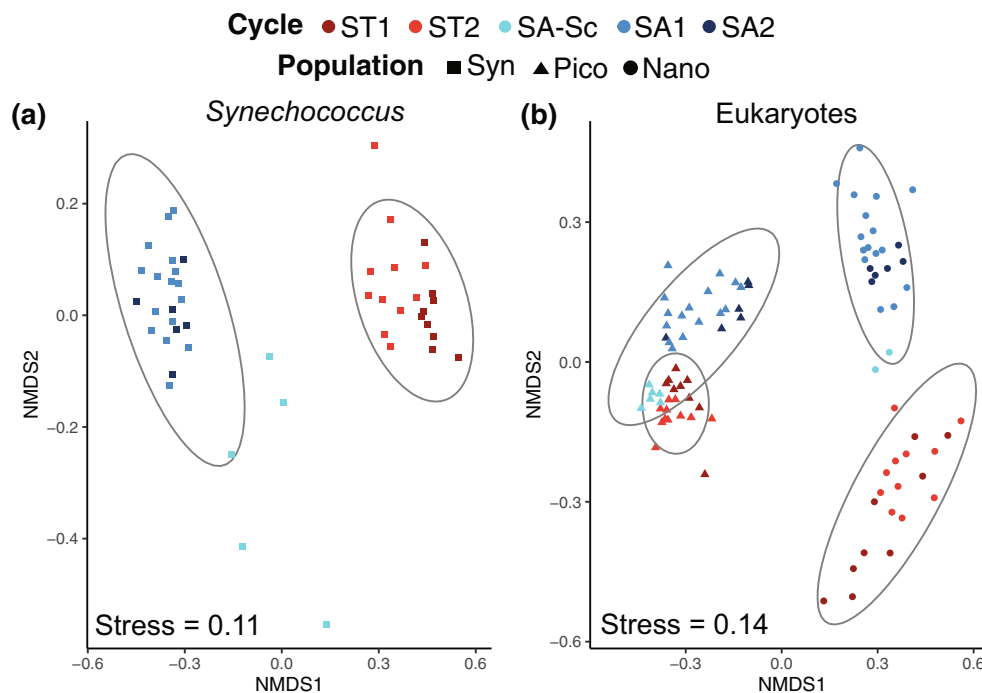


Fig. 3. Non-metric multidimensional scaling (NMDS) of flow cytometry sorted (a) *Synechococcus petB* community and (b) photosynthetic picoeukaryote and nanoeukaryote 18S rRNA community. Each point corresponds to one sample. Samples are colored by cycle and shapes denote *Synechococcus* (Syn), picoeukaryotes (Pico), and nanoeukaryotes (Nano). Ellipses correspond to water mass (subtropical or subantarctic).

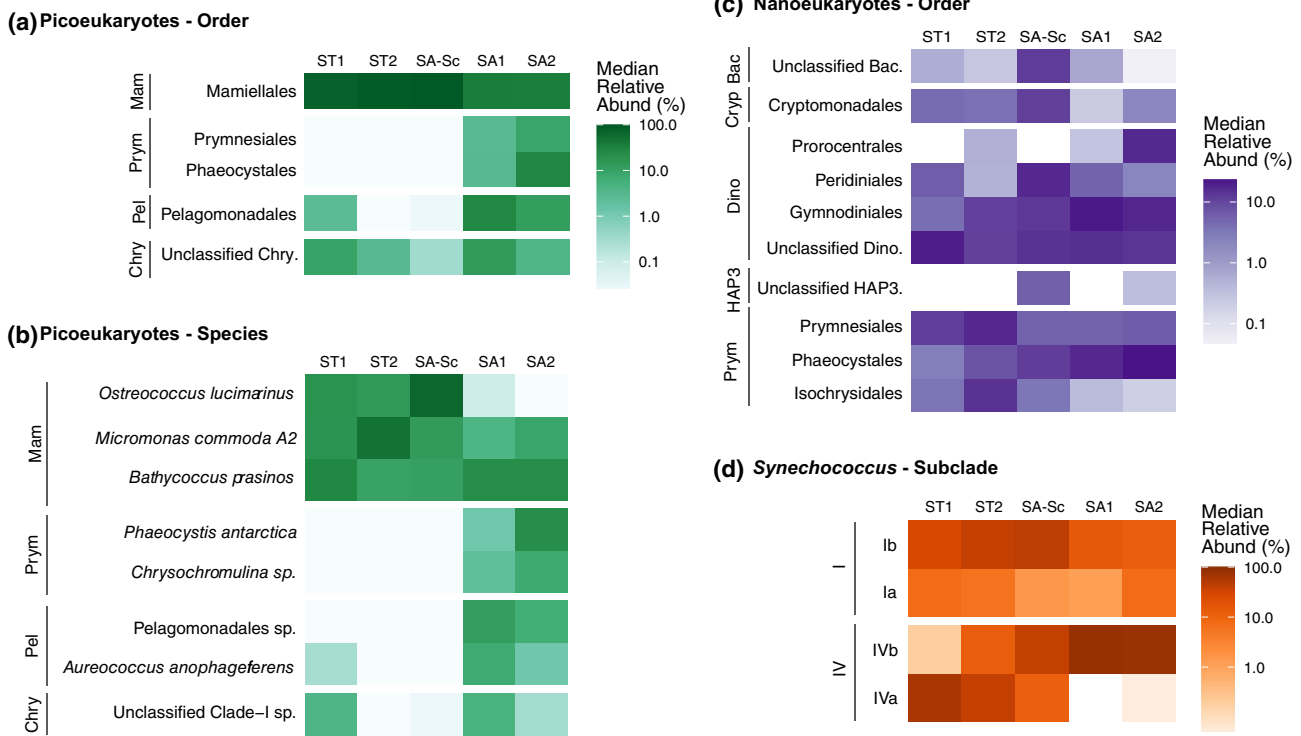


Fig. 4. Median relative abundance (%) of reads in each cycle for flow cytometry sorted populations, only including taxa that have a median relative abundance higher than 5% within each sorted population in at least one cycle. Picoeukaryotes at (a) order and (b) species level, (c) Nanoeukaryotes at order level, and (d) *Synechococcus* at subclade level. Samples are ordered from left to right across a spatial gradient, from subtropical (ST) to subantarctic (SA) cycles. Taxa are grouped by class for eukaryotes: Mamiellophyceae (Mam), Prymnesiophyceae (Prym), Pelagophyceae (Pel), Chrysophyceae (Chry), Bacillariophyta (Bac), Cryptophyceae (Cryp), Dinophyceae (Dino), and Haptophyta Clade HAP3 (HAP3), and clades for *Synechococcus*: I and IV.

excluding SA-Sc where the picoeukaryotic component was nearly completely dominated by Mamiellophyceae (97.5%). The median relative abundance of Pelagophyceae and Prymnesiophyceae in picoeukaryote samples increased from 0% in subtropical cycles to 18.9% and 14.4% in subantarctic cycles, respectively. Chrysophyceae had similar median relative abundance across subtropical and subantarctic water masses (4.4% and 6.7%, respectively). *Phaeocystis antarctica* (Prymnesiophyceae) dominated in SA2 with median relative abundance of 24.6% (Fig. 4b).

Among photosynthetic nanoeukaryotes, Dinophyceae (60.5%) and Prymnesiophyceae (30.3%) were the most abundant classes. The composition of Dinophyceae at order level changed from subtropical to subantarctic cycles (Fig. 4c). The proportion of unclassified Dinophyceae reads was higher in subtropical cycles, Peridinales were more abundant in SA-Sc, while Gymnodinales (mostly *Karodinium* sp.) and Prorocentrales (*Prorocentrum* sp.) increased in abundance in oceanic subantarctic cycles (Fig. S13). Among Prymnesiophyceae, Isochrysidales (only *Gephyrocapsa huxleyi*) and Prymnesiales reads were more abundant in subtropical cycles (median relative abundance of 8.8% and 15.7%, respectively), while Phaeocystales (mainly *Phaeocystis antarctica*)

reads were more abundant in subantarctic cycles (17.7%; Figs. 4c, S13). *Phaeocystis antarctica* (corresponding to the same ASV) and *Chrysochromulina* sp. (corresponding to different ASVs) were the only abundant taxa present in both pico- and nanoeukaryote samples. Bacillariophyta, Cryptomonadales, and Haptophyta clade HAP3 were present in lower abundance and increased in proportion in SA-Sc (12.2%, 11.3%, and 5.8%, respectively; Fig. 4c).

We classified the ASVs present in the sorted pico and nanoeukaryote populations as phototrophic or phago-mixotrophic (Table S5). For picoeukaryotes, the median relative abundance of phago-mixotrophic taxa increased in oceanic subantarctic cycles to 47.2% in SA2 (Fig. 5a). For nanoeukaryotes, phago-mixotrophic taxa dominated nearly all the cycles (50.7%–70.4%) except SA-Sc (32.4%; Fig. 5b).

Sorted *Synechococcus* was dominated by subclades Ia, Ib, IVa, and IVb of clades I and IV, accounting for 99.98% of total reads (Fig. 4d). Clade IV had a higher median relative abundance compared to clade I (65.8% vs. 34.2%). Subclade IVa was more dominant in subtropical cycles (46.9%) while IVb was more dominant in subantarctic cycles (74.4%).

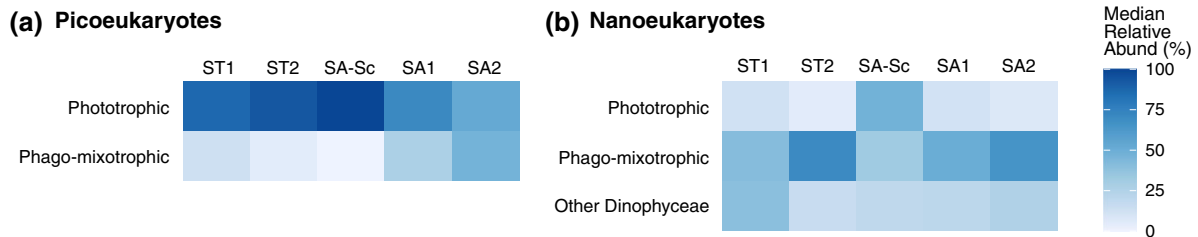


Fig. 5. Median relative abundance (%) of reads in each cycle for flow cytometry sorted eukaryotic populations classified based on trophic mode. (a) Picoeukaryote and (b) nanoeukaryote ASVs classified as phototrophic or phago-mixotrophic (taxa that express, or have potential to express, phototrophy and phagotrophy, sensu Mitra et al. 2023). The category “other Dinophyceae” are Dinophyceae taxa that are unclassified, and therefore unable to be assigned a trophic mode.

To validate our approach, we compared the relative abundance of taxa (ASVs) found in the sorted populations with their relative abundance in the total community. The community composition of sorted *Synechococcus*, and picoeukaryotes and nanoeukaryotes were similar in relative abundance to filtered seawater samples (Tables S8–S10), indicating that the populations sorted by flow cytometry after ¹⁴C incubations were not distorted. The one exception was picoeukaryotes, with Chlorophyceae (primarily *Chloroparvula pacifica*) showing higher relative abundance in filtered (12%) compared to sorted (1.3%) samples of oceanic subantarctic cycles (Table S9).

Discussion

High contribution of small phytoplankton toward productivity in the subtropical frontal zone

Small phytoplankton (pico and nano size fractions; Richardson 2019) were important contributors to photosynthetic biomass in the subtropical frontal zone during the austral spring (Décima et al. 2023), which align with previous measurements in the region (McKay et al. 2005) and highlight the important contribution of small phytoplankton even under productive conditions (Barber and Hiscock 2006; Gutiérrez-Rodríguez et al. 2023). The phytoplankton community in oceanic subantarctic cycles (SA1 and SA2) were likely iron-limited, as indicated by lower photochemical efficiency of photosystem II (Fv/fm) and higher reoxidation kinetics (Q_a^- lifetime) compared to subtropical cycles (Décima et al. 2023, Fig. 2c, corresponding to “Salp SA” and “Non-salp SA” cycles) consistent with physiological evidence from subantarctic waters of this region (Boyd et al. 1999). Under nutrient-limited conditions, smaller phytoplankton have greater nutrient affinity and lower transport limitation for macronutrients (Raven 1998) and micronutrients (Hudson and Morel 1990) over larger phytoplankton. Smaller cells are also hypothesized to be less sensitive to iron-limited conditions due to lower iron quotas (Barber and Hiscock 2006).

Compared to oceanic subantarctic cycles, the coastal SA-Sc cycle had higher relative contribution of microphytoplankton to Chl *a* biomass and NPP, as well as higher Fv/fm and lower Q_a^- lifetime values. This suggests an alleviation of HNLC

conditions in SA-Sc stations, possibly due to the influence of the Southland Current, as described in Décima et al. (2023).

Comparable variation of cell-specific carbon fixation rates with the literature

Despite the variation in cell-specific carbon fixation rates between some replicates or experiments of the same cycle (Fig. S3), these rates were consistent with the range and group-specific trends reported in previous studies (Fig. 6). The high variation in carbon fixation rates from single-cell measurements (Duerschlag et al. 2021; Irion et al. 2021) suggests that part of the variation we observed likely reflects true biological variability intrinsic to natural population dynamics and its adaptive capability to diverse environmental conditions (Olofsson et al. 2019). Moreover, the systematically lower cell-specific carbon fixation rates exhibited by *Synechococcus* followed by photosynthetic pico- and nanoeukaryotes in both subtropical and subantarctic cycles, has been reported in warmer tropical (Grob et al. 2011; Jardillier et al. 2010; Zubkov 2014) and colder Antarctic regions (Irion et al. 2021; Fig. 6), reinforcing the consistent size-dependent pattern.

Synechococcus and picoeukaryotes cell-specific carbon fixation rates were on the lower end of previously published rates (Fig. 6). This was particularly marked for *Synechococcus* rates measured in subantarctic waters. Previous studies mostly measured cell-specific carbon fixation rates across oligotrophic and mesotrophic conditions (Table S11), while this study was conducted mainly in oligotrophic conditions with low macronutrient concentrations in subtropical waters (surface mixed layer $NO_3 \approx 1 \mu M$; Fig. S10E), or low iron concentrations in subantarctic waters, which could have capped cell-specific carbon fixation rates (Rii et al. 2016; Duerschlag et al. 2021). Additionally, this study was conducted at a higher latitude with lower sea surface temperatures (up to 15°C difference, excluding Irion et al. 2021), which possibly contributed to the lower cell-specific carbon fixation rates and growth rates of this study (Chen et al. 2014; Hartmann et al. 2014).

In contrast, the cell-specific carbon fixation rates of nanoeukaryotes in our study were within the same range of values as reported by the only other study measuring rates

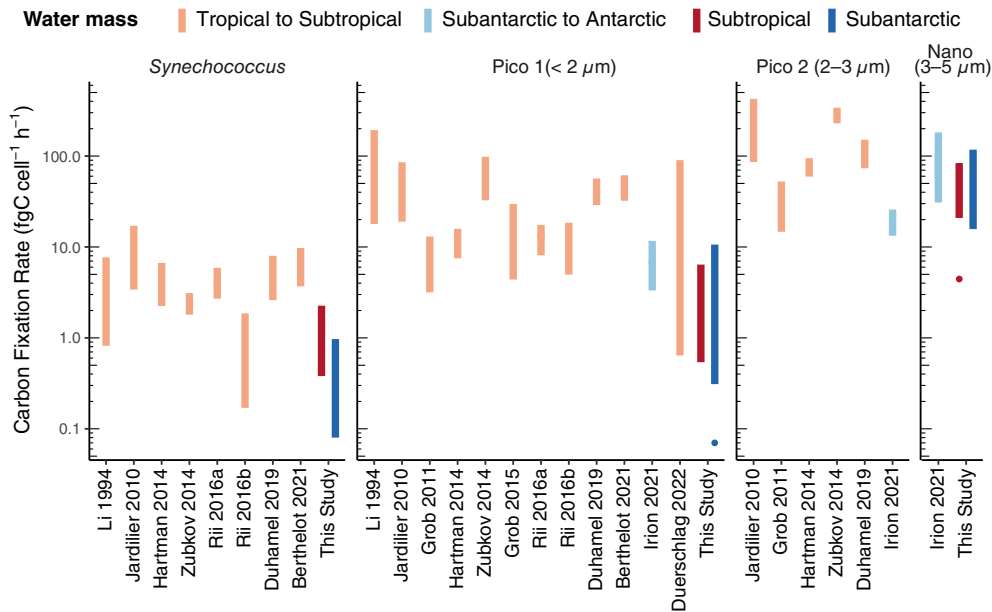


Fig. 6. Range of cell-specific/single-cell phytoplankton productivity rates ($\text{fgC cell}^{-1} \text{h}^{-1}$) from previous measurements compared to this study. Phytoplankton populations include *Synechococcus* and small eukaryotes of three size groups: Pico 1 (average cell diameter $< 2 \mu\text{m}$), Pico 2 ($2\text{--}3 \mu\text{m}$), and Nano ($3\text{--}5 \mu\text{m}$). Colors indicate water mass. Points indicate outliers in this study. A complete summary is provided in Table S11.

of nanoeukaryotes in the Southern Ocean (Fig. 6; Irion et al. 2021).

Variation of cell-specific carbon fixation rates and the associated community across water masses

The influence of taxonomic affiliation on cell-specific carbon fixation rates is often overlooked (Rii et al. 2016; Duhamel et al. 2019). We assessed the taxonomic composition of the small phytoplankton populations of different domains (picocyanobacteria and eukaryotes) and sizes (pico and nano) in ^{14}C -fixation experiments with flow cytometry sorting and DNA metabarcoding. Metabarcoding of sorted populations revealed distinct community composition between subtropical and subantarctic waters for each phytoplankton group, as well as between pico- and nanoeukaryote populations (Fig. 3). There were no significant differences in cell size between subtropical and subantarctic cycles for any of the three groups (Table S7), nor was light likely a limiting factor (as daily incidence irradiance and depth-profile PAR were similar between the water masses; Figs. S1, S10C). Therefore, the differences in cell-specific carbon fixation rates between warm, macronutrient-limited subtropical cycles, and colder, iron-limited subantarctic cycles were likely a reflection of intrinsic carbon-based growth rates affected by temperature (Chen et al. 2014) and nutrient availability (Rii et al. 2016; Irion et al. 2021), as well as taxa-specific responses (Caputi et al. 2019; Villiot et al. 2023).

The cell-specific carbon fixation rates and growth rates of photosynthetic pico- and nanoeukaryotes did not significantly differ between the water masses (Fig. 2a,c), suggesting changes

in sea surface temperature and nutrient-limited conditions had no significant influence on these rates of small photosynthetic eukaryotes in this study. This trend is consistent with the growth rates of picoeukaryotes from dilution experiments in the same area (Safi et al. 2023). We did not expect temperature change in this study to affect the rates of small eukaryotes. The change in sea surface temperature (3°C) between the cycles was smaller than the ranges shown to affect eukaryotic phytoplankton growth (Marañón et al. 2014), if they were even observed (Landry et al. 2022). Moreover, most of the taxa present in both cycles are abundant or have high growth rates in temperatures that are similar or colder than that of subantarctic conditions (Irion et al. 2020; Gutiérrez-Rodríguez et al. 2023). While no study has directly compared the cell-specific carbon fixation rates of small phytoplankton across macronutrient-limited and iron-limited conditions, a comparison between iron-limited and nutrient-replete conditions in the Southern Ocean suggested lower carbon-based growth rates for picoeukaryotes but not nanoeukaryotes (see Irion et al. 2021, based on interquartile range of cell-specific growth rates).

The sorted picoeukaryote community in subantarctic cycles (Prymnesiophyceae and Chrysophyceae) and nanoeukaryote community in both subtropical and subantarctic cycles (Dinophyceae and Prymnesiophyceae) were dominated by taxa with reported phago-mixotrophic strategies (taxa that express, or have potential to express, phototrophy and phagotrophy, sensu Mitra et al. 2023; Figs. 4a,b, 5). The picoeukaryote community in subantarctic waters contained phago-mixotrophic Prymnesiophyceae and Chrysophyceae

taxa, which are abundant in the HNLC Southern Ocean region, and known to be adapted to low iron conditions (Irion et al. 2020; Gutiérrez-Rodríguez et al. 2023). In contrast, the picoeukaryotic community in subtropical and coastal SA-Sc cycles was dominated by phototrophic Mamiellophyceae, which are an important component of marine phytoplankton communities in moderately oligotrophic open ocean conditions (Gutiérrez-Rodríguez et al. 2022).

The picoeukaryote Chloropicophyceae (primarily *Chloroparvula pacifica*) was abundant in the filtered samples of subantarctic cycles in this study and in HNLC subantarctic waters of the same region (Gutiérrez-Rodríguez et al. 2022), but underrepresented in sorted samples (Table S9). The underestimation of Chloropicophyceae in the sorted community is likely due to unsuccessful cell preservation, as the prevalence of Chloropicophyceae in open ocean waters was originally described from live sorted populations (Moon-van der Staay et al. 2001). Nevertheless, at least two chloropicophycean strains are proposed as phago-mixotrophic (Bock et al. 2021).

Within the nanoeukaryote community, the relative abundance of Dinophyceae could have been overestimated due to high copy number of ribosomal RNA (Zhu et al. 2005). However, its presence was also indicated by the significant contribution of Peridinin to total Chl *a* biomass (2%–6%) in Décima et al. (2023). Taxa within the major orders (Peridiniales, Gymnodiniales, and Prorocentrales) and genera (*Karodinium* and *Prorocentrum*) of Dinophyceae identified in our sorted dataset have been recorded as mixotrophic (Schneider et al. 2020; Mitra et al. 2023). Unfortunately, a good proportion of Dinophyceae reads (15.1%) and ASVs (11%) lacked formal description, which impairs their assignment to trophic modes. The distribution of dominant Prymnesiophyceae species present in the nanoeukaryote community (*Gephyrocapsa huxleyi*, *Chrysochromulina* sp., and *Phaeocystis antarctica*) was consistent with previous studies (Gutiérrez-Rodríguez et al. 2022). These taxa have been proposed as phago-mixotrophic through experimental evidence (Li et al. 2022) and gene-based model predictions (Koppelle et al. 2022). This study used flow cytometry sorting for detailed resolution of proposed phago-mixotrophic taxa relative abundance, which was key in detecting differences in proportion of phago-mixotrophic taxa in pico and nanoeukaryote populations. These differences could not be identified in the mixoplankton global distribution map presented in Mitra et al. (2023).

The similar cell-specific carbon fixation rates for small photosynthetic eukaryotes between the water masses might be sustained by phago-mixotrophic strategy being deployed among the taxa described in our samples. While mixotrophy via osmotrophy is likely a ubiquitous trait among phytoplankton (as discussed in Mitra et al. 2023), phago-mixotrophy is a specific characteristic that can vary at genera level (Schneider et al. 2020). Phago-mixotrophy can increase the competitiveness of mixoplankton under macro and micronutrient-limited conditions by alleviating nutrient stress (Zubkov and

Tarran 2008; Stukel et al. 2011), possibly through using prey-derived nutrients to supplement or maintain photosynthetic carbon fixation (Arenovski et al. 1995; Mitra and Flynn 2023). Small mixoplankton flagellates (3–5 μm) carry out at least 40% of bacterivory in oligotrophic and HNLC conditions (Zubkov and Tarran 2008; Stukel et al. 2011). Duhamel et al. (2019) reported that small eukaryotes (< 5 μm), where Dinophyceae were present, had low phosphate uptake in oligotrophic conditions despite high biomass-normalized carbon fixation rates. The authors suggested phago-mixotrophy as a way for small eukaryotes to overcome macronutrient limitation. Using a trait-based approach, we observed taxa with proposed phago-mixotrophic strategies present in distinct pico and nanoeukaryote populations in iron-limited conditions, and in nanoeukaryote populations under macronutrient-limited conditions. Based on this observation, we suggest that the consistent cell-specific carbon fixation rates by small photosynthetic eukaryotes across contrasting nutrient regimes could be due to the presence of phago-mixotrophy to overcome iron limitation for picoeukaryotes, and both macronutrient and iron limitation for nanoeukaryotes.

At SA-Sc, where iron limitation was likely alleviated, the proportion of phototrophic taxa increased but the cell-specific carbon fixation rates and group-specific productivity for pico and nanoeukaryotes remained similar compared to oceanic subantarctic cycles. This suggests that alleviating nutrient limitation could reduce the presence of phago-mixotrophic taxa (Arenovski et al. 1995) while not affecting productivity, supporting our hypothesis.

Other adaptations to low iron conditions besides phago-mixotrophy were also likely present in the community of subantarctic cycles. *Bathycoccus prasinos*, Pelagophyceae, and *Phaeocystis antarctica* are suggested to have a physiological advantage in iron uptake and/or storage (Simmons et al. 2016; Luxem et al. 2017; Guérin et al. 2022). *Phaeocystis antarctica* was the only taxa present in both picoeukaryote and nanoeukaryote populations represented by the same ASV, which could be due to a size reduction response under iron limitation (Luxem et al. 2017). Additionally, manganese and vitamin B1 might also be limiting factors in subantarctic waters (Bertrand et al. 2007; Latour et al. 2023). Manganese limitation affects the growth of small phytoplankton, although this is suggested to occur later during summer (Latour et al. 2023). Vitamin B1 limitation affects the growth of Mamiellophyceae which rely on exogenous sources (Paerl et al. 2015).

In contrast to small eukaryotes, *Synechococcus* had a decrease in cell-specific carbon fixation rates and growth rates from subtropical to subantarctic cycles (Fig. 2), consistent with the growth rate patterns obtained with serial dilution experiments during the same sampling cruise (Gutiérrez-Rodríguez unpubl.), and in another study measured in the same region (Safi et al. 2023). This could be partly due to cold-adapted clades I and IV (Fig. 4d; Farrant et al. 2016) having lower growth

rates under subantarctic temperature conditions, as the growth rate of *Synechococcus* is tightly coupled to temperature (Hunter-Cevera et al. 2020; Landry et al. 2022). Additionally, the optimal temperature for growth of clade I strains (22°C) is higher than their original environment (10–15°C), suggesting some cold-adapted clades are not true psychrophilic phytoplankton (Pittera et al. 2014).

Changes in the community composition of *Synechococcus* from subtropical to subantarctic cycles suggested a shift toward ecotypes described in, and therefore possibly adapted to, low iron conditions. The environmental niche of *Synechococcus* at subclade level is not yet well-defined, but the distribution of subclades seems to exhibit environmental preferences (Farrant et al. 2016). Farrant et al. (2016) suggest subclade IVa (corresponding to Ecologically Significant Taxonomic Unit [ESTU] IVA) thrives in cold conditions where iron is not limiting, consistent with its dominance in subtropical cycles in this study. While there is no agreement on the niche of subclade IVb (ESTU IVC in Farrant et al. 2016), its high relative abundance in subantarctic cycles indicates that it is at least tolerant of iron-limited conditions. Whole genome analysis found siderophore uptake genes in clade IV (Hogle et al. 2022), suggesting clade IV can adapt to low iron conditions by directly taking up siderophore-bound iron instead of dissolved iron. Yet, the low cell-specific carbon fixation rates and growth rates of this group observed in HNLC waters might indicate that *Synechococcus* populations were iron-stressed in subantarctic cycles, which has been suggested to happen even among *Synechococcus* communities with adaptations to low iron conditions (Gilbert et al. 2022).

Although *Synechococcus* had lower cell-specific carbon fixation rates in subantarctic compared to subtropical waters, its group-specific productivity was not significantly different between the water masses due to higher cell abundance in subantarctic waters. The greater accumulation of *Synechococcus* in subantarctic compared to subtropical waters, despite lower growth rates, could be the result of a decoupling between growth and loss rates during the spring bloom (Hunter-Cevera et al. 2020). As lower temperature is associated with lower grazing (Rose and Caron 2007) and viral lysis rates (Mojica et al. 2016), *Synechococcus* could have lower loss rates in subantarctic waters compared to subtropical waters, leading to a greater accumulation. Alternatively, *Synechococcus* might have high standing stock in the region as it had similar abundance at the nearby Bounty Trough region (47° S and 170° E) during autumn (Gutiérrez-Rodríguez et al. 2020), when growth and loss rates are expected to re-couple after its decoupling during spring and summer periods (Hunter-Cevera et al. 2020).

Growth rates reported in this study are within the same range as those reported in previous studies using isotope uptake measurements (Duerschlag et al. 2021; Irion et al. 2021). It is important to note that the growth rates rely on cellular carbon biomass measurements reported in the literature (Menden-Deuer and Lessard 2000; Bertilsson et al. 2003)

that can range by an order of magnitude, across spatial scales and taxonomic composition (Buitenhuis et al. 2012).

In conclusion, small phytoplankton contributed to a large proportion of phytoplankton biomass and primary production across oligotrophic subtropical to HNLC subantarctic waters in the southwest Pacific Ocean. Although *Synechococcus* had lower cell-specific carbon fixation rates in HNLC subantarctic compared to subtropical waters, the group-specific productivity remained the same due to high cell abundance. Pico- and nanoeukaryote populations had no significant difference in cell-specific carbon fixation rates despite changes from macro to micronutrient-limited conditions. A closer look at the taxonomic composition suggests taxa with reported phagomixotrophic capabilities might use this trophic strategy to adapt to contrasting nutrient-limited conditions. Additional in situ measurements of phagotrophy by phagomixoplankton (Zubkov and Tarran 2008) paired with taxonomic identification (Li et al. 2022) are needed to better assess the contribution of phago-mixotrophic populations toward carbon-fixation, especially in nutrient-limited conditions.

Data availability statement

Source code (all sequence processing and analysis scripts) for this paper is available on Github (https://github.com/deniseong/TAN1810_C14). All unprocessed sequencing data have been deposited in NCBI Sequence Read Archive (*petB* (filtered and sorted samples)—PRJNA885274, 18SV4 (filtered samples)—PRJNA670061 and PRJNA1033349 (Table S4), 18SV4 (sorted samples)—PRJNA1033349). Raw data files from flow cytometry sorting are available on <http://flowrepository.org> (Repository ID: FR-FCM-Z5P8) and metadata for data files are available on <https://github.com/deniseong/marine-Synechococcus-metaB>.

References

- Arenovski, A. L., E. L. Lim, and D. A. Caron. 1995. Mixotrophic nanoplankton in oligotrophic surface waters of the Sargasso Sea may employ phagotrophy to obtain major nutrients. *J. Plankton Res.* **17**: 801–820. doi:10.1093/plankt/17.4.801
- Barber, R. T., and M. R. Hiscock. 2006. A rising tide lifts all phytoplankton: Growth response of other phytoplankton taxa in diatom-dominated blooms. *Global Biogeochem. Cycles* **20**: GB4S03. doi:10.1029/2006GB002726
- Berthelot, H., S. Duhamel, S. L'Helguen, J.-F. Maguer, S. Wang, I. Cetinić, and N. Cassar. 2019. NanoSIMS single cell analyses reveal the contrasting nitrogen sources for small phytoplankton. *ISME J.* **13**: 651–662. doi:10.1038/s41396-018-0285-8
- Bertilsson, S., O. Berglund, D. M. Karl, and S. W. Chisholm. 2003. Elemental composition of marine *Prochlorococcus* and *Synechococcus*: Implications for the ecological stoichiometry

- of the sea. *Limnol. Oceanogr.* **48**: 1721–1731. doi:10.4319/lo.2003.48.5.1721
- Bertrand, E. M., M. A. Saito, J. M. Rose, C. R. Riesselman, M. C. Lohan, A. E. Noble, P. A. Lee, and G. R. DiTullio. 2007. Vitamin B12 and iron colimitation of phytoplankton growth in the Ross Sea. *Limnol. Oceanogr.* **52**: 1079–1093. doi:10.4319/lo.2007.52.3.1079
- Bock, N. A., S. Charvet, J. Burns, Y. Gyaltshen, A. Rozenberg, S. Duhamel, and E. Kim. 2021. Experimental identification and in silico prediction of bacterivory in green algae. *ISME J.* **15**: 1987–2000. doi:10.1038/s41396-021-00899-w
- Boyd, P., J. LaRoche, M. Gall, R. Frew, and R. M. L. McKay. 1999. Role of iron, light, and silicate in controlling algal biomass in subantarctic waters SE of New Zealand. *J. Geophys. Res.: Oceans* **104**: 13395–13408. doi:10.1029/1999JC900009
- Buitenhuis, E. T., and others. 2012. Picophytoplankton biomass distribution in the global ocean. *Earth Syst. Sci. Data* **4**: 37–46. doi:10.5194/essd-4-37-2012
- Callahan, B. J., P. J. McMurdie, M. J. Rosen, A. W. Han, A. J. A. Johnson, and S. P. Holmes. 2016. DADA2: High-resolution sample inference from Illumina amplicon data. *Nat. Methods* **13**: 581–583. doi:10.1038/nmeth.3869
- Caputi, L., and others. 2019. Community-level responses to iron availability in open ocean plankton ecosystems. *Global Biogeochem. Cycles* **33**: 391–419. doi:10.1029/2018GB006022
- Chen, B., H. Liu, B. Huang, and J. Wang. 2014. Temperature effects on the growth rate of marine picoplankton. *Mar. Ecol. Prog. Ser.* **505**: 37–47. doi:10.3354/meps10773
- Décima, M., and others. 2023. Salp blooms drive strong increases in passive carbon export in the Southern Ocean. *Nat. Commun.* **14**: 425. doi:10.1038/s41467-022-35204-6
- Duerschlag, J., and others. 2021. Niche partitioning by photosynthetic plankton as a driver of CO₂-fixation across the oligotrophic South Pacific Subtropical Ocean. *ISME J.* **16**: 465–476. doi:10.1038/s41396-021-01072-z
- Duhamel, S., E. Kim, B. Sprung, and O. R. Anderson. 2019. Small pigmented eukaryotes play a major role in carbon cycling in the P-depleted western subtropical North Atlantic, which may be supported by mixotrophy. *Limnol. Oceanogr.* **64**: 2424–2440. doi:10.1002/lno.11193
- Farrant, G. K., and others. 2016. Delineating ecologically significant taxonomic units from global patterns of marine picocyanobacteria. *Proc. Natl. Acad. Sci. U. S. A.* **113**: E3365–E3374. doi:10.1073/pnas.1524865113
- Field, C. B., M. J. Behrenfeld, J. T. Randerson, and P. Falkowski. 1998. Primary production of the biosphere: Integrating terrestrial and oceanic components. *Science* **281**: 237–240. doi:10.1126/science.281.5374.237
- Flynn, R. F., L. Haraguchi, J. McQuaid, J. M. Burger, P. Mutseka Lunga, L. Stirnimann, S. Samanta, A. N. Roychoudhury, and S. E. Fawcett. 2023. Nanoplankton: The dominant vector for carbon export across the Atlantic Southern Ocean in spring. *Sci. Adv.* **9**: eadi3059. doi:10.1126/sciadv.adi3059
- Garcia, N., P. Raimbault, and V. Sandroni. 2007. Seasonal nitrogen fixation and primary production in the Southwest Pacific: Nanoplankton diazotrophy and transfer of nitrogen to picoplankton organisms. *Mar. Ecol. Prog. Ser.* **343**: 25–33. doi:10.3354/meps06882
- Gérikas Ribeiro, C., A. Lopes dos Santos, D. Marie, F. Pereira Brandini, and D. Vaultot. 2018. Small eukaryotic phytoplankton communities in tropical waters off Brazil are dominated by symbioses between Haptophyta and nitrogen-fixing cyanobacteria. *ISME J.* **12**: 1360–1374. doi:10.1038/s41396-018-0050-z
- Gilbert, N. E., G. LeClerc, R. F. Strzepek, M. J. Ellwood, B. S. Twining, S. Roux, C. Pennacchio, P. W. Boyd, and S. W. Wilhelm. 2022. Bioavailable iron titrations reveal oceanic *Synechococcus* ecotypes optimized for different iron availabilities. *ISME Commun.* **2**: 1–12. doi:10.1038/s43705-022-00132-5
- Grob, C., M. Hartmann, M. V. Zubkov, and D. J. Scanlan. 2011. Invariable biomass-specific primary production of taxonomically discrete picoeukaryote groups across the Atlantic Ocean. *Environ. Microbiol.* **13**: 3266–3274. doi:10.1111/j.1462-2920.2011.02586.x
- Guérin, N., and others. 2022. Genomic adaptation of the picoeukaryote *Pelagomonas calceolata* to iron-poor oceans revealed by a chromosome-scale genome sequence. *Commun. Biol.* **5**: 1–14. doi:10.1038/s42003-022-03939-z
- Guillou, L., and others. 2013. The Protist ribosomal reference database (PR2): A catalog of unicellular eukaryote small sub-unit rRNA sequences with curated taxonomy. *Nucleic Acids Res.* **41**: D597–D604. doi:10.1093/nar/gks1160
- Gutiérrez-Rodríguez, A., and others. 2020. Decoupling between phytoplankton growth and microzooplankton grazing enhances productivity in subantarctic waters on Campbell plateau, southeast of New Zealand. *J. Geophys. Res.: Oceans* **125**: e2019JC015550. doi:10.1029/2019JC015550
- Gutiérrez-Rodríguez, A., and others. 2022. Planktonic protist diversity across contrasting subtropical and Subantarctic waters of the southwest Pacific. *Prog. Oceanogr.* **206**: 102809. doi:10.1016/j.pocean.2022.102809
- Gutiérrez-Rodríguez, A., M. Latasa, K. Safi, M. H. Pinkerton, and S. D. Nodder. 2023. Decoupled growth and grazing rates of diatoms and green algae drive increased phytoplankton productivity on HNLC sub-Antarctic plateaux. *Limnol. Oceanogr. Lett.* **8**: 896–905. doi:10.1002/lol2.10355
- Hartmann, M., P. Gomez-Pereira, C. Grob, M. Ostrowski, D. J. Scanlan, and M. V. Zubkov. 2014. Efficient CO₂ fixation by surface *Prochlorococcus* in the Atlantic Ocean. *ISME J.* **8**: 2280–2289. doi:10.1038/ismej.2014.56
- Hogle, S. L., T. Hackl, R. M. Bundy, J. Park, B. Satinsky, T. Hiltunen, S. Biller, P. M. Berube, and S. W. Chisholm. 2022. Siderophores as an iron source for picocyanobacteria

- in deep chlorophyll maximum layers of the oligotrophic ocean. *ISME J.* **16**: 1636–1646. doi:10.1038/s41396-022-01215-w
- Hudson, R. J. M., and F. M. M. Morel. 1990. Iron transport in marine phytoplankton: Kinetics of cellular and medium coordination reactions. *Limnol. Oceanogr.* **35**: 1002–1020. doi:10.4319/lo.1990.35.5.1002
- Hunter-Cevera, K. R., M. G. Neubert, R. J. Olson, A. Shalapyonok, A. R. Solow, and H. M. Sosik. 2020. Seasons of Syn. *Limnol. Oceanogr.* **65**: 1085–1102. doi:10.1002/lno.11374
- Irion, S., L. Jardillier, I. Sassenhagen, and U. Christaki. 2020. Marked spatiotemporal variations in small phytoplankton structure in contrasted waters of the Southern Ocean (Kerguelen area). *Limnol. Oceanogr.* **65**: 2835–2852. doi:10.1002/lno.11555
- Irion, S., U. Christaki, H. Berthelot, S. L'Helguen, and L. Jardillier. 2021. Small phytoplankton contribute greatly to CO₂-fixation after the diatom bloom in the Southern Ocean. *ISME J.* **15**: 2509–2522. doi:10.1038/s41396-021-00915-z
- Jardillier, L., M. V. Zubkov, J. Pearman, and D. J. Scanlan. 2010. Significant CO₂ fixation by small prymnesiophytes in the subtropical and tropical northeast Atlantic Ocean. *ISME J.* **4**: 1180–1192. doi:10.1038/ismej.2010.36
- Koppelle, S., D. López-Escardó, C. P. D. Brussaard, J. Huisman, C. J. M. Philippart, R. Massana, and S. Wilken. 2022. Mixotrophy in the bloom-forming genus *Phaeocystis* and other haptophytes. *Harmful Algae* **117**: 102292. doi:10.1016/j.hal.2022.102292
- Landry, M. R., K. E. Selph, R. R. Hood, C. H. Davies, and L. E. Beckley. 2022. Low temperature sensitivity of picophytoplankton P : B ratios and growth rates across a natural 10°C temperature gradient in the oligotrophic Indian Ocean. *Limnol. Oceanogr. Lett.* **7**: 112–121. doi:10.1002/lo2.10224
- Latour, P., and others. 2023. Seasonality of phytoplankton growth limitation by iron and manganese in subantarctic waters. *Elem. Sci. Anth.* **11**: 00022. doi:10.1525/elementa.2023.00022
- Laufkötter, C., and others. 2015. Drivers and uncertainties of future global marine primary production in marine ecosystem models. *Biogeosciences* **12**: 6955–6984. doi:10.5194/bg-12-6955-2015
- Li, W. K. W. 1994. Primary production of prochlorophytes, cyanobacteria, and eucaryotic ultraphytoplankton: Measurements from flow cytometric sorting. *Limnol. Oceanogr.* **39**: 169–175. doi:10.4319/lo.1994.39.1.0169
- Li, Q., K. F. Edwards, C. R. Schvarcz, and G. F. Steward. 2022. Broad phylogenetic and functional diversity among mixotrophic consumers of *Prochlorococcus*. *ISME J.* **16**: 1557–1569. doi:10.1038/s41396-022-01204-z
- Litchman, E., P. de Tezanos Pinto, C. A. Klausmeier, M. K. Thomas, and K. Yoshiyama. 2010. Linking traits to species diversity and community structure in phytoplankton. *Hydrobiologia* **653**: 15–28. doi:10.1007/s10750-010-0341-5
- Logares, R., and others. 2020. Disentangling the mechanisms shaping the surface ocean microbiota. *Microbiome* **8**: 55. doi:10.1186/s40168-020-00827-8
- Luxem, K. E., M. J. Ellwood, and R. F. Strzeppek. 2017. Intraspecific variability in *Phaeocystis antarctica*'s response to iron and light stress. *PLoS One* **12**: e0179751. doi:10.1371/journal.pone.0179751
- Marañón, E., P. Cermeño, M. Huete-Ortega, D. C. López-Sandoval, B. Mouriño-Carballido, and T. Rodríguez-Ramos. 2014. Resource supply overrides temperature as a controlling factor of marine phytoplankton growth. *PLoS One* **9**: e99312. doi:10.1371/journal.pone.0099312
- Marie, D., X. L. Shi, F. Rigaut-Jalabert, and D. Vaultot. 2010. Use of flow cytometric sorting to better assess the diversity of small photosynthetic eukaryotes in the English Channel. *FEMS Microbiol. Ecol.* **72**: 165–178. doi:10.1111/j.1574-6941.2010.00842.x
- McKay, R. M. L., S. W. Wilhelm, J. Hall, D. A. Hutchins, M. M. D. al-Rshaidat, C. E. Mioni, S. Pickmere, D. Porta, and P. W. Boyd. 2005. Impact of phytoplankton on the biogeochemical cycling of iron in subantarctic waters southeast of New Zealand during FeCycle. *Global Biogeochem. Cycles* **19**: GB4S24. doi:10.1029/2005GB002482
- Menden-Deuer, S., and E. J. Lessard. 2000. Carbon to volume relationships for dinoflagellates, diatoms, and other protist plankton. *Limnol. Oceanogr.* **45**: 569–579. doi:10.4319/lo.2000.45.3.0569
- Mitra, A., and K. J. Flynn. 2023. Low rates of bacterivory enhances phototrophy and competitive advantage for mixoplankton growing in oligotrophic waters. *Sci. Rep.* **13**: 6900. doi:10.1038/s41598-023-33962-x
- Mitra, A., and others. 2023. The Mixoplankton database (MDB): Diversity of photo-phago-trophic plankton in form, function, and distribution across the global ocean. *J. Eukaryotic Microbiol.* **70**: e12972. doi:10.1111/jeu.12972
- Mojica, K. D. A., J. Huisman, S. W. Wilhelm, and C. P. D. Brussaard. 2016. Latitudinal variation in virus-induced mortality of phytoplankton across the North Atlantic Ocean. *ISME J.* **10**: 500–513. doi:10.1038/ismej.2015.130
- Moon-van der Staay, S. Y., R. De Wachter, and D. Vaultot. 2001. Oceanic 18S rDNA sequences from picoplankton reveal unsuspected eukaryotic diversity. *Nature* **409**: 607–610. doi:10.1038/35054541
- Moore, J., and others. 2018. Sustained climate warming drives declining marine biological productivity. *Science* **359**: 113–1143. doi:10.1126/science.aao6379
- Obiol, A., C. R. Giner, P. Sánchez, C. M. Duarte, S. G. Acinas, and R. Massana. 2020. A metagenomic assessment of microbial eukaryotic diversity in the global ocean. *Mol. Ecol. Resour.* **20**: 718–731. doi:10.1111/1755-0998.13147
- Olofsson, M., O. Kourtchenko, E.-M. Zetsche, H. K. Marchant, M. J. Whitehouse, A. Godhe, and H. Ploug. 2019. High

- single-cell diversity in carbon and nitrogen assimilations by a chain-forming diatom across a century. *Environ. Microbiol.* **21**: 142–151. doi:[10.1111/1462-2920.14434](https://doi.org/10.1111/1462-2920.14434)
- Ong, D. R. Y., A. Gutiérrez-Rodríguez, L. Garczarek, D. Marie, and A. Lopes dos Santos. 2023. Nested PCR approach for petB gene metabarcoding of marine *Synechococcus* populations. *Microbiol. Spectr.* **0**: e04086-22. doi:[10.1128/spectrum.04086-22](https://doi.org/10.1128/spectrum.04086-22)
- Paerl, R. W., E. M. Bertrand, A. E. Allen, B. Palenik, and F. Azam. 2015. Vitamin B1 ecophysiology of marine picoeukaryotic algae: Strain-specific differences and a new role for bacteria in vitamin cycling. *Limnol. Oceanogr.* **60**: 215–228. doi:[10.1002/lno.10009](https://doi.org/10.1002/lno.10009)
- Piredda, R., M. P. Tomasino, A. M. D'Erchia, C. Manzari, G. Pesole, M. Montresor, W. H. C. F. Kooistra, D. Sarno, and A. Zingone. 2017. Diversity and temporal patterns of planktonic protist assemblages at a Mediterranean Long Term Ecological Research site. *FEMS Microbiol. Ecol.* **93**: fiw200. doi:[10.1093/femsec/fiw200](https://doi.org/10.1093/femsec/fiw200)
- Pittera, J., F. Humily, M. Thorel, D. Grulois, L. Garczarek, and C. Six. 2014. Connecting thermal physiology and latitudinal niche partitioning in marine *Synechococcus*. *ISME J.* **8**: 1221–1236. doi:[10.1038/ismej.2013.228](https://doi.org/10.1038/ismej.2013.228)
- Raven, J. A. 1998. The twelfth Tansley lecture. Small is beautiful: The picophytoplankton. *Funct. Ecol.* **12**: 503–513. doi:[10.1046/j.1365-2435.1998.00233.x](https://doi.org/10.1046/j.1365-2435.1998.00233.x)
- Richardson, T. L. 2019. Mechanisms and pathways of small-phytoplankton export from the surface ocean. *Ann. Rev. Mar. Sci.* **11**: 57–74. doi:[10.1146/annurev-marine-121916-063627](https://doi.org/10.1146/annurev-marine-121916-063627)
- Rii, Y. M., S. Duhamel, R. R. Bidigare, D. M. Karl, D. J. Repeta, and M. J. Church. 2016. Diversity and productivity of photosynthetic picoeukaryotes in biogeochemically distinct regions of the South East Pacific Ocean. *Limnol. Oceanogr.* **61**: 806–824. doi:[10.1002/lno.10255](https://doi.org/10.1002/lno.10255)
- Rose, J. M., and D. A. Caron. 2007. Does low temperature constrain the growth rates of heterotrophic protists? Evidence and implications for algal blooms in cold waters. *Limnol. Oceanogr.* **52**: 886–895. doi:[10.4319/lo.2007.52.2.0886](https://doi.org/10.4319/lo.2007.52.2.0886)
- Ryan-Keogh, T. J., S. J. Thomalla, P. M. S. Monteiro, and A. Tagliabue. 2023. Multidecadal trend of increasing iron stress in Southern Ocean phytoplankton. *Science* **379**: 834–840. doi:[10.1126/science.abc5237](https://doi.org/10.1126/science.abc5237)
- Safi, K. A., A. G. Rodríguez, J. A. Hall, and M. H. Pinkerton. 2023. Phytoplankton dynamics, growth and microzooplankton grazing across the subtropical frontal zone, east of New Zealand. *Deep-Sea Res. II Top. Stud. Oceanogr.* **208**: 105271. doi:[10.1016/j.dsr2.2023.105271](https://doi.org/10.1016/j.dsr2.2023.105271)
- Schneider, L., and others. 2020. A dataset on trophic modes of aquatic protists. *Biodivers. Data J.* **8**: e56648. doi:[10.3897/BDJ.8.e56648](https://doi.org/10.3897/BDJ.8.e56648)
- Selph, K. E. 2021. Enumeration of marine microbial organisms by flow cytometry using near-UV excitation of Hoechst 34580-stained DNA. *Limnol. Oceanogr.: Methods* **19**: 692–701. doi:[10.1002/lom3.10454](https://doi.org/10.1002/lom3.10454)
- Sim, C. W. H., C. G. Ribeiro, F. L. Gall, I. Probert, P. Gourvil, C. Lovejoy, D. Vaultot, and A. L. dos Santos. 2024. Temporal dynamics and biogeography of sympagic and planktonic autotrophic microbial eukaryotes during the under-ice Arctic bloom. *bioRxiv* **26**: 591324. doi:[10.1101/2024.04.26.591324](https://doi.org/10.1101/2024.04.26.591324)
- Simmons, M. P., S. Sudek, A. Monier, A. J. Limardo, V. Jimenez, C. R. Perle, V. A. Elrod, J. T. Pennington, and A. Z. Worden. 2016. Abundance and biogeography of picoprasinophyte ecotypes and other phytoplankton in the eastern north Pacific Ocean. *Appl. Environ. Microbiol.* **82**: 1693–1705. doi:[10.1128/AEM.02730-15](https://doi.org/10.1128/AEM.02730-15)
- Stukel, M. R., M. R. Landry, and K. E. Selph. 2011. Nanoplankton mixotrophy in the eastern equatorial Pacific. *Deep-Sea Res. II* **58**: 378–386. doi:[10.1016/j.dsr2.2010.08.016](https://doi.org/10.1016/j.dsr2.2010.08.016)
- Stukel, M. R., M. Décima, K. E. Selph, and A. Gutiérrez-Rodríguez. 2021. Size-specific grazing and competitive interactions between large salps and protistan grazers. *Limnol. Oceanogr.* **66**: 2521–2534. doi:[10.1002/lno.11770](https://doi.org/10.1002/lno.11770)
- Vaultot, D., W. Eikrem, M. Viprey, and H. Moreau. 2008. The diversity of small eukaryotic phytoplankton ($\leq 3 \mu\text{m}$) in marine ecosystems. *FEMS Microbiol. Rev.* **32**: 795–820. doi:[10.1111/j.1574-6976.2008.00121.x](https://doi.org/10.1111/j.1574-6976.2008.00121.x)
- Villiot, N., A. E. Maas, A. J. Poulton, and L. Blanco-Bercial. 2023. Organic and inorganic nutrients modulate taxonomic diversity and trophic strategies of small eukaryotes in oligotrophic oceans. *FEMS Microbes* **4**: xtac029. doi:[10.1093/femsmc/xtac029](https://doi.org/10.1093/femsmc/xtac029)
- Zentara, S.-J., and D. Kamykowski. 1981. Geographic variations in the relationship between silicic acid and nitrate in the South Pacific Ocean. *Deep-Sea Res. A: Oceanogr. Res. Pap.* **28**: 455–465. doi:[10.1016/0198-0149\(81\)90137-0](https://doi.org/10.1016/0198-0149(81)90137-0)
- Zhu, F., R. Massana, F. Not, D. Marie, and D. Vaultot. 2005. Mapping of picoeukaryotes in marine ecosystems with quantitative PCR of the 18S rRNA gene. *FEMS Microbiol. Ecol.* **52**: 79–92. doi:[10.1016/j.femsec.2004.10.006](https://doi.org/10.1016/j.femsec.2004.10.006)
- Zubkov, M. V. 2014. Faster growth of the major prokaryotic versus eukaryotic CO₂ fixers in the oligotrophic ocean. *Nat. Commun.* **5**: 3776. doi:[10.1038/ncomms4776](https://doi.org/10.1038/ncomms4776)
- Zubkov, M. V., and G. A. Tarran. 2008. High bacterivory by the smallest phytoplankton in the North Atlantic Ocean. *Nature* **455**: 224–226. doi:[10.1038/nature07236](https://doi.org/10.1038/nature07236)

Acknowledgments

We acknowledge the crew of RV *Tangaroa* for their efforts during the TAN1810 voyage. We thank Daniel Vaultot (CNRS, France) for providing the equation to calculate cell-specific carbon fixation rate and feedback on data processing. We are grateful to Jaret Bilewicz and Debbie Hulston (NIWA, New Zealand) for the sample processing support. We thank Molly A. Moynihan (Marine Biological Laboratory) for guidance into rates and field measurements. We are grateful to Eleanor Slade and Ong Xin Rui (NTU, Singapore) for providing invaluable guidance on statistical analysis.

Ong *et al.*

DRYO and ALS were supported by RG91/21 and RG26/19 Singapore Ministry of Education, Academic Research Fund Tier 1. AG-R was supported by NIWA via the New Zealand Ministry of Business, Innovation and Employment's Strategic Science Investment Funding to the National Coasts Ocean Centre. KES was supported by NSF award OCE-1756610.

Conflict of Interest

None declared.

Small phytoplankton ¹⁴C-fixation cell rates

Submitted 04 April 2024

Revised 17 August 2024

Accepted 09 November 2024

Associate Editor: Takuhei Shiozaki